Article

Journal of Nanoscience and Nanotechnology
Vol. 15, 9473–9481, 2015
www.aspbs.com/jnn

Synthesis and Characterization of Bimetallic $Ni_{50}Pt_{50}$ Catalyst Supported on SiO_2 for N_2O Decomposition

A. Ángeles-Pascual[1], R. Esparza[2,*], O. Téllez-Vazquez[2], S. Velumani[1], and R. Pérez[2]

[1] Centro de Investigación y de Estudios Avanzados del I.P.N., Av. Instituto Politécnico Nacional 2508 Col. San Pedro Zacatenco, México D.F., 07360, México

[2] Centro de Física Aplicada y Tecnología Avanzada, Universidad Nacional Autónoma de México, Boulevard Juriquilla 3001, Santiago de Querétaro, Qro., 76230, México

Nanometallic and bimetallic catalyst of Ni, Pt and $Ni_{50}Pt_{50}$ were studied by the decompositions of N_2O. The catalyst were prepared by incipient wetness impregnation of the silica with low superficial area of 50 m^2/g supported with aqueous solution of the metal precursors, for Pt $H_2Pt\ Cl_6 \cdot 6H_2O$ was used and for Ni, $Ni(NO_3)_2$ was used to a total metal loading of 1% wt. Catalyst were oxidized for 2 hours at 400 °C with O_2, then the samples were reduced for 30 minutes with N_2 and 2 hours with H_2, all at the same temperature. The catalyst was characterized by Transmission Electron Microscopy (TEM), High Angular Annular Dark Field (HAADF), High Resolution Transmission Electron Microscopy (HR-TEM) and Termoprogramed Reduction (TPR). The mean particle sizes obtained by TEM and HAADF were about 12.5 nm for Ni/SiO_2, 2.8 nm for Pt/SiO_2 and 3.5 nm $Ni_{50}Pt_{50}/SiO_2$ catalysts respectability. HR-TEM and HAADF analysis showed differences between Ni and Pt catalysts displaying mainly cuboctahedral shapes. Stepped surface defects were found in the $Ni_{50}Pt_{50}/SiO_2$ catalyst. Finally $Ni_{50}Pt_{50}/SiO_2$ was more active than Pt/SiO_2 and Ni/SiO_2 catalysts for the decomposition of N_2O.

Keywords: Bimetallic Nanoparticles, Structural Determination, Scanning/Transmission Electron Microscopy, Corrected-Aberration, Decomposition, Molecular Simulation.

1. INTRODUCTION

Supported bimetallic catalysts have been given great attention because have proven to be important materials for many catalytic applications,[1,2] in particular the Ni–Pt system is well known for exhibiting properties that are distinctly different from those of the corresponding monometallic catalyst, nowadays they play significant roles in combating pollution,[3,4] specially decomposition of N_2O precursor of greenhouse gas.[5–7] The addition of a transition metal to active metals not only enhances catalytic reactivity but also induces changes in selectivity with high resistance to deactivation compared to monometallic catalyst.[8]

Many investigations combining experimental studies and theoretical calculations,[9,10] have been performed with the aim to correlate electronic properties of bimetallic surface catalysts, in particular the platinum and nickel system because it exhibits different catalytic and reducibility properties and these metals are active in a great number of processes of practical importance.[11,12] The Ni–Pt system can improve the methanol oxidation by lowering the electronic binding energy in Pt and the presence of NiO in the catalyst provides an oxygen sources for CO_2 oxidation[13] and lower potential. The Pt/Ni bimetallic nanoparticles supported on ZrO_2 have also been employed for reactions such as reduction for hydrogenation of benzene,[14] the adsorption and decomposition of ethylene,[15] the decomposition of N_2O, the selective hydrogenation of acetylene in the presence of ethylene.[16,17] Other systems such as Pt/Cu, have been studied for the conversion of *n*-butane to iso-butane,[18] while Pt–Ru subjected to H_2, CO, N_2 and air atmosphere is used for fuel cell catalysts.[19] The bifunctional catalysts can be used to replace those catalysts associated with high costs, and also can provide additional selectivity and conversion to targeted products.

In more recent studies, it has been demonstrated that the structure of the bimetallic surfaces also plays a

*Author to whom correspondence should be addressed.

 1533-4880/2015/15/9473/009 doi:10.1166/jnn.2015.10200

significant role in controlling their electronic and catalytic properties.[20] The better catalytic performance of core–shell Ni–Pt nanoparticles could be related to near surface alloy effects where subsurface metal and alloys layers affect the binding of adsorbents to the particles surface.[21] Thus, for example, the Ni/Pt (111) bimetallic surface with Ni coverage at one monolayer (ML), the Ni atoms can reside either on the surface to produce a Ni–terminated Ni–Pt (111) surface or in the surface region to form a Pt-terminated Pt–Ni–Pt (111) surface structure.[22, 23] Theoretical and experimental studies show that the ML Pt–Ni–Pt (111) structure is very active toward the hydrogenation of the C═C bonds, this phenomenon could be related with the decomposition of N_2O. The core–shell Ni/Ag led to an increase in catalytic surface area of Ni, in consequence a sharp increase in catalytic activity and selectivity is obtained. The core–shell Ni–Pt nanoparticles are ideal structures for improve catalytic reactivity[24] and also, has been found that the alloys composition Pt–Ni had notably catalytic activity.[25] The main objective of this work is to get an insight of the different crystalline phases in the catalysts, understand its surface characteristics and describe how they affect the catalytic properties of the supported bimetallic nanoparticles. The second objective is to determine the efficiency of decomposition of N_2O. To achieve these objectives, Ni–Pt bimetallic nanoparticles were synthesized applying time–temperature–atmosphere treatments to incipient wetness impregnated metal-salt precursor. The catalyst was characterized by corrected- aberration scanning/transmission electron microscopy (STEM), high-annular angle dark-field (HAADF) and high–resolution transmission electron microscopy (HR–TEM). Surface characteristics of the samples were investigated using dynamic flow such as H_2 temperature programmed reduction (H_2-TPR) analysis and the catalytic activity was evaluated via N_2O decomposition.

2. EXPERIMENTAL PROCEDURE

2.1. Materials

The Ni, Pt and the Ni–Pt catalysts were supported on SiO_2 Degussa with low surface area $S = 50$ m^2/g. The total metal loading was 1% wt and the atomic composition of the monometallic catalysts was at $Ni/SiO_2 = 1$, $Pt/SiO_2 = 1$ and the bimetallic catalyst was $Ni/Pt = 1$ denoted as $Ni_{50}Pt_{50}/SiO_2$. The $Ni(NO_3)_2 \cdot 6H_2O$ (Aldrich) and $H_2PtCl_6 \cdot 6H_2O$ (Merck) were used as chemical precursors in the synthesis of the bimetallic catalysts, then for reduction of the catalysts, H_2 pure was used and N_2O was used for the catalytic activity evaluation.

2.2. Catalysts Preparation

The Ni–Pt bimetallic catalysts supported on SiO_2 were prepared by incipient wetness impregnation method.[26] The support was immersed in an aqueous solution containing the desired concentration of Ni and Pt as metallic precursors. After drying at 358 K during 12 h to remove the wetness, the samples were calcined in flowing air 60 ml^3/min at 673 K for 4.5 h and then were purged in flowing of nitrogen gas at the same temperature; finally the samples were reduced in pure H_2 at the same temperature and for the same period of time.

2.3. Catalyst Characterization

To characterize the NiPt catalyst, copper grids with carbon film were prepared with a drop of the solution. The samples were analyzed using aberration-corrected (Cs) scanning transmission electron microscopy (STEM) with a Jeol ARM200F (200 keV) FEG-TEM/STEM, equipped with a CEOS Cs corrector on the illumination system.

High-resolution transmission electron microscopy (HR-TEM) and high-angle annular dark field (HAADF)-STEM images were obtained. The probe current used in STEM mode was 23.2 pA using a condenser lens aperture size of 40 microns. The HAADF-STEM images were registered using a camera length of 80 mm and a collection angle of 50–180 mrad. Elemental analysis was performed using X-ray energy-dispersive spectroscopy (EDS, Oxford). HR-TEM image simulations have been performed using the SimulaTEM software package[27] which uses the multislice algorithm.[28] The parameters considered for the simulation correspond to the experimental conditions of the microscope.

2.4. Molecular Dynamics

Molecular dynamics (MD) simulations were used to model the behavior of the Ni, Pt and NiPt particles. The cuboctahedral structure with 490 atoms was the approximate model of the particles observed in the electron microscopy.

The simulation was performed based on the canonical ensemble (NVT) using the XenoView program. The time step used to perform the simulation was 2.6 nanosecond (ns). Periodic boundary conditions were applied in all the directions of the simulation cell. A slope of temperature from 300 at 1400 K was used. The Consistent Force Field (CFF)[29] where the potential energy is calculated as a sum of interatomic potentials was used.

2.5. Thermo Programmed Reductions (TPR)

The calcined and reduced samples were placed in the quartz reactor previously dried with oxygen at room temperature at a rate a 283 K/min until 1073 K for 1 h, after the quartz reactor was left to cool at room temperature, 100 mg of catalyst was deposited inside the quartz reactor and then treated at rate of 283 K/min in the presence of 5% H_2/Ar gas mixture to reach 1073 K, while the H_2 consumption was monitoring for termed conductivity detector (TCD) *in situ,* and then for cooling, inert gas as Argon was used. The experiment was done

in multitask characterization unit RIG-100 from *In-Situ* Research Experiments Inc.

2.6. Catalytic Activity

The reactivity of the catalysts was studied in the decomposition using N_2O as a probe. This decomposition reaction was studied in the range of temperature from 300–1100 K working at atmospheric pressure. The amount of sample used of each catalyst Ni/SiO_2, Pt/SiO_2 and $Ni_{50}Pt_{50}/SiO_2$ were 100 mg. They were put inside the quartz reactor, then these were reactivated with H_2 at room temperature at rate of 30 ml^3/min to reach 1073 K for 1 h,[26] then the samples were cooled and purged at low temperature with pure Helium flow. From room temperature, the temperature is increased supplying the N_2O gas for decomposition and at each increment of temperature the catalytic activity was evaluated according to:

$$\%N_2O = \frac{[(N_2O)_{in} - (N_2O)_{out}]}{[(N_2O)_{in}]}(100\%)$$

Where: $(N_2O)_{in}$ and $(N_2O)_{out}$ are the N_2O concentration in and out.

The reactions products in the decomposition N_2O were analyzed by a gas chromatography Porapaq Q using 4-m packed Chromosorb column, coupled to the output of the reactor.

3. RESULTS AND DISCUSSION

The morphology of catalysts was studied using scanning transmission electron microscopy (STEM) analysis in mode of high-angle annular dark field (HAADF). Figure 1 shows the typical images of the Ni, Pt and $Ni_{50}Pt_{50}$ bimetallic catalyst and their particle size distribution. All the particles have good dispersion on the supported silica and similar morphologies are observed in each catalyst. The average particles sizes of the nanoparticles are 12.5 nm, 2.8 nm and 3.5 nm for Ni, Pt and $Ni_{50}Pt_{50}$ catalyst respectively. The distribution histograms indicate that the Ni particles have a wide size distribution due to the agglomeration of smaller metal particles. This agglomeration could be related with the formation of a layer of oxide surrounding the surface metal,[30] this oxidation occurred during the preparation of catalyst and contact with the environment. The histograms of the Pt and $Ni_{50}Pt_{50}$ catalysts show a narrow size distribution. A comparisons of the average particles sizes shows that the Ni nanoparticles are approximately five times larger than the Pt and $Ni_{50}Pt_{50}$, this could be attributed to the contact with the environment, which promotes the oxidation and particles agglomeration forming some phyllosilicates of Ni.[31] As can observed in the histograms, the size of particles decrease with the increase in Pt content, this phenomenon may be explained as due to the decrease in the total number of atoms available in the catalyst during the oxidation, reduction and growth process. A small average size nanoparticle could affect the reactivity of the catalysts due to the variation in active surface available for reaction. It is important to mention that all the nanoparticles have good wettability with the silica support. This phenomenon represents a strong interaction between the support and the metallic phase.[1]

Figure 2 shows the high-resolution transmission electron microscopy (HR-TEM) images of Ni/SiO_2 and Pt/SiO_2 catalyst. Figure 2(a) shows a HR-TEM image of Ni/SiO_2 particle, where d-spacing 0.204 nm was obtained. Such d-spacing correspond to (111) crystalline plane of the Ni face-centered-cubic crystal structure with $a_0 = 0.3523$ nm and space group Fm-3 m (JPDF 04-0850). As can be observed before, the Ni particles had regular morphologies with an average size of 12.5 nm; the morphology of the particles is similar to a cuboctahedral shape. Figure 2(b) shows the theoretically-simulated HR-TEM image and the model of Ni particle with cuboctahedral shape, the image is simulated along the [123] crystalline orientation. The comparison between the experimental and simulated images suggests the possible nature of the atomistic structural configuration. Figure 2(c) shows a typical HR-TEM image of a Pt/SiO_2 particle, where d-spacings 0.225, 0.225 and 0.194 nm were obtained. Such d-spacings correspond to (1–11), (11–1) and (200) crystalline plane of the Pt face-centered-cubic crystal structure with $a_0 = 0.3923$ nm and space group Fm-3 m (JPDF 04-0802). Similar to Ni/SiO_2 particles, the Pt/SiO_2 showed regular morphologies especially with cuboctahedral shapes. Figure 2(d) shows a theoretical HR-TEM simulated image and the model of Pt particle with cuboctahedral shape, the simulated image is oriented along the [011] crystalline axis and it is agreed with the experimental image. As can be observed, the simulated images of the Ni and Pt are almost similar to the experimental HR-TEM images. Most of the particles were founded covered or surrounded by silica, it could be related with the strong interaction metal/support as has been reported in the literature,[32] even some nanoparticles showed planes which are more active sites than others.

Figure 3 shows a series of electron microscopy images of $Ni_{50}Pt_{50}/SiO_2$ particles. Figure 3(a) shows a HR-TEM image with its corresponding fast Fourier transform (FFT) where measurements of the d-spacings 0.2154, 0.216 and 0.1955 nm were obtained. Such d-spacings correspond to (11-1), (1-1-1) and (020) crystalline planes of the NiPt tetragonal crystal structure[33] with $a_0 = 0.3821$ and $c_0 = 0.3591$ nm and space group P4/mmm (JPDF 65-9446) and the particle is oriented in the [101] zone axis. Figure 3(b) shows a HAADF-STEM image with its corresponding FFT of a particle oriented in the [001] zone axis. The measurements of the d-spacings 0.269, 0.193, 0.190, and 0.1341 nm correspond to (1–10), (020), (200) and (220) crystalline planes of the NiPt tetragonal crystal structure. In this figure is clearly observed the contrast of the atoms,

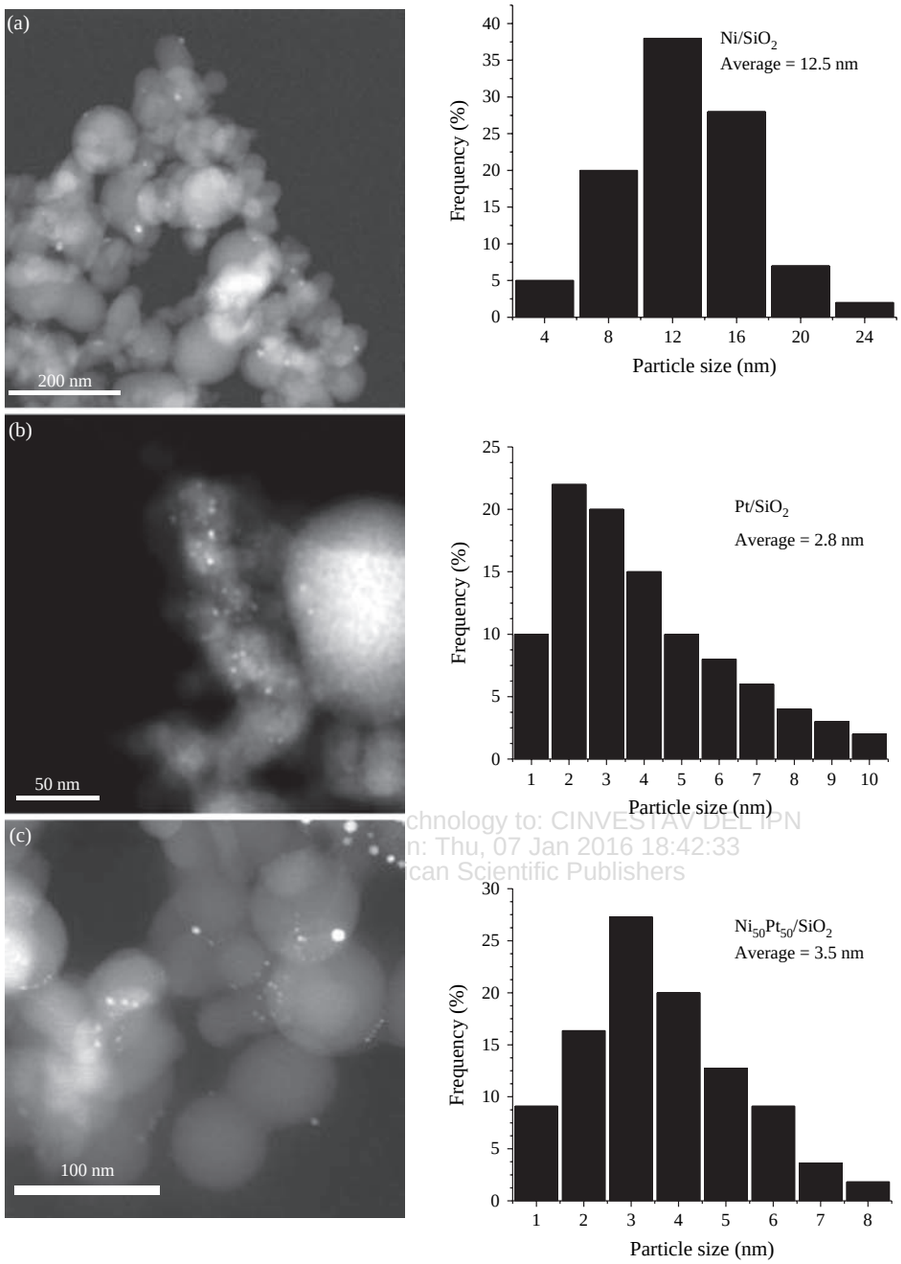

Figure 1. STEM images and particle size histograms of: (a) Ni/SiO_2, (b) Pt/SiO_2 and (c) $Ni_{50}Pt_{50}/SiO_2$.

where the strong brightness dots correspond to the Pt and the weak brightness dots correspond to the Ni. Therefore this particle could be related with a cuboctahedral shape with Pt and Ni atoms randomly disordered forming an alloy. Usually the structure more reported of the NiPt is $L1_0$ type in the Strukturbericht notation, which is an ordered structure,[34] however, in our case the NiPt forms a disordered alloy. The cuboctahedral shape of the NiPt particles is the responsible of enhanced behavior for the decomposition of the N_2O, because of the {111} planes are more active than the others.[26] Therefore, nanoparticles with the same sizes and showing {111} planes could be more active and its properties could help in the catalytic activity for this specific case. The type of atoms on the planes are very important for the subsequent properties, thus, in the structure type alloy, the atoms are mixed; this arrangement of atoms changes the structure and catalytic properties of the $Ni_{50}Pt_{50}/SiO_2$ catalyst. Figure 1(c) shows an energy-dispersive spectrum (EDS) of the elemental composition of the $Ni_{50}Pt_{50}/SiO_2$ catalyst. The EDS shows the presence of Si, O, Ni and Pt (Cu is associated with the grid). The elemental composition of the Ni and

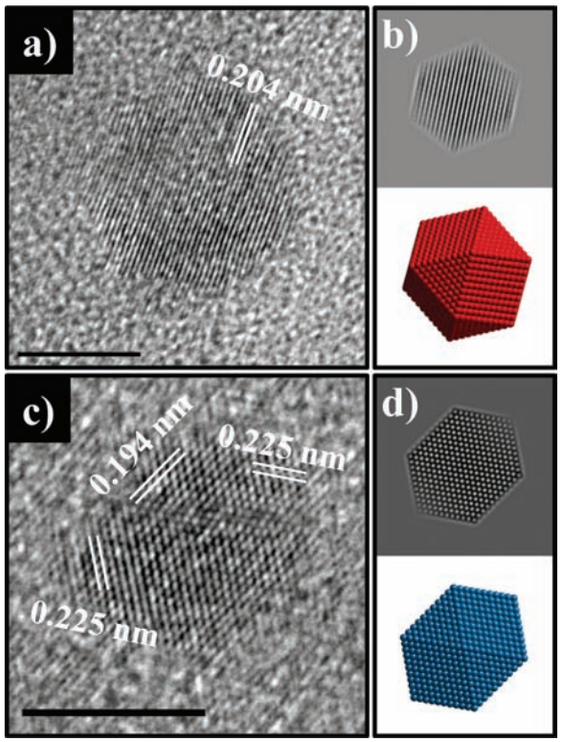

Figure 2. HR-TEM images of Ni/SiO_2 and Pt/SiO_2 catalysts. (a) Ni particle with regular shape, (b) simulated image and model of Ni particle, (c) HR-TEM image of Pt particle and (d) simulated image and model of Pt particle.

Pt shows a ratio atomic close to 1:1, which confirms the obtained results by electron microscopy, that the particles are related with a tetragonal structure with a composition $Ni_{50}Pt_{50}$.

STEM combined with EDS (STEM-EDS) is one of the most widely used techniques for performing microanalysis of the nanomaterials.[35] The analysis of the distribution of the Ni and Pt elements from the $Ni_{50}Pt_{50}/SiO_2$ catalyst were obtained. Figure 4(a) shows a HAADF– STEM image of the $Ni_{50}Pt_{50}/SiO_2$ catalyst indicating the region of the elemental analysis, the variation of the contrast in the image is associated with the NiPt particle covered or surrounded by SiO_2. In this case only the Ni and Pt elements were analyzed. Figure 4(b) shows the STEM-EDS line-scan across the $Ni_{50}Pt_{50}/SiO_2$ catalyst. The Ni-Kα and the Pt-Lα signals were traced across the region of the individual particle with the maximum intensity of the signals. As can be observed, the signals are almost similar in intensity along the different regions of the particle, which indicate that both elements are located random in the particle with the same composition.

Figure 5(a) shows a HAADF-STEM image of the $Ni_{50}Pt_{50}/SiO_2$ catalyst. From the image and its FFT measurements of the d-spacings 0.2183, 0.2146 and 0.1917 nm corresponding to (11-1), (1-1-1) and (020) crystalline planes of the NiPt tetragonal crystal structure were

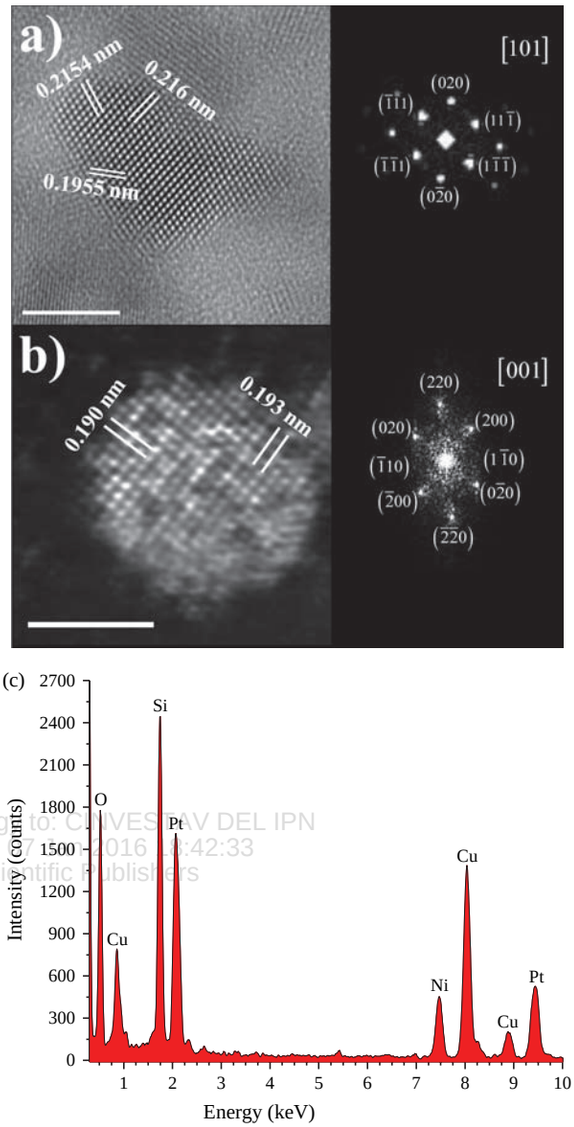

Figure 3. (a) HR-TEM image with its FFT of $Ni_{50}Pt_{50}/SiO_2$ catalyst showing distances in the [101] orientation, (b) HAADF-STEM image with its FFT of $Ni_{50}Pt_{50}/SiO_2$ catalyst showing distances in the [001] orientation, (c) EDS spectrum from the $Ni_{50}Pt_{50}/SiO_2$ catalyst.

obtained. The particle is oriented in the [101] zone axis and has morphology similar to cuboctahedron truncated. A special characteristic in this particle is that {020} crystalline planes have stepped surface defects. These defects not only have a strong influence on the particle growth but also on the reactivity and much of the surface chemistry carried out of nanomaterials are related to these defects.[36] The stepped surface defects are considered as high energy facets and it has been demonstrated that they may be present on the surfaces of the polyhedral morphologies.[37] It is due to that polyhedral structures can produce more kink interfaces (or atomic steps) than spherical ones. Figure 5(b) shows the HAADF-STEM image

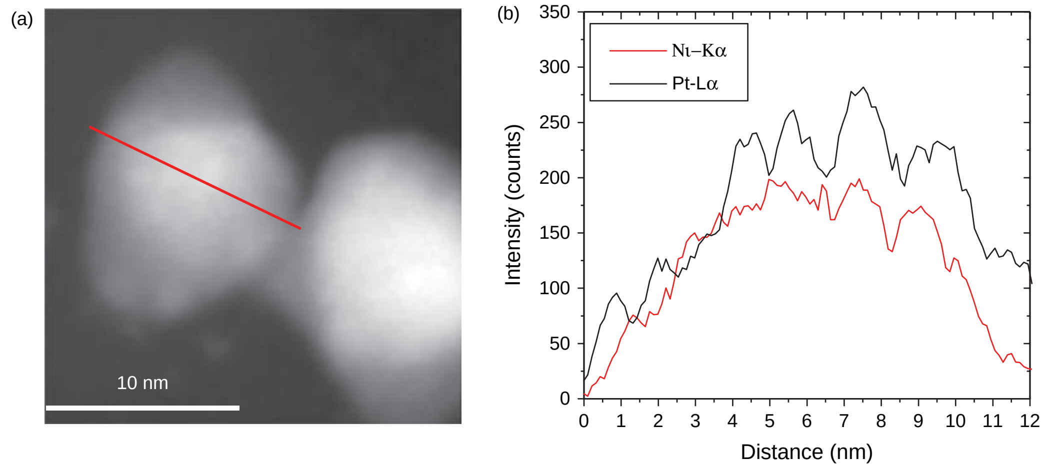

Figure 4. STEM-EDS elemental analysis by line-scan across the $Ni_{50}Pt_{50}/SiO_2$ catalyst. (a) HAADF-STEM image of the corresponding $Ni_{50}Pt_{50}/SiO_2$ catalyst and (b) Elemental Ni and Pt line profiles, the overlapping indicates homogeneous alloy distribution in the catalysts.

with color look-up, which is useful for highlighting subtle intensity variations. In this image is clear the contrast of the elements, where it is possible appreciate that an amorphous layer of SiO_2 is surrounding the NiPt particle. This indicates the good wettability of the particles on the substrate.

In order to obtain more information about the HAADF-STEM image of the Figure 5(a), and also, that allows us to identify areas where the Pt and Ni are located, a statistical analysis of the atomic column intensities was carried out. Figure 5(c) shows a color map representing integrated intensity of the atoms; the intensity of the signal from atomic column in the raw image has been integrated and plotted using Absolute Integrator v1.2. The intensity variation in HAADF-STEM images is due to Rutherford

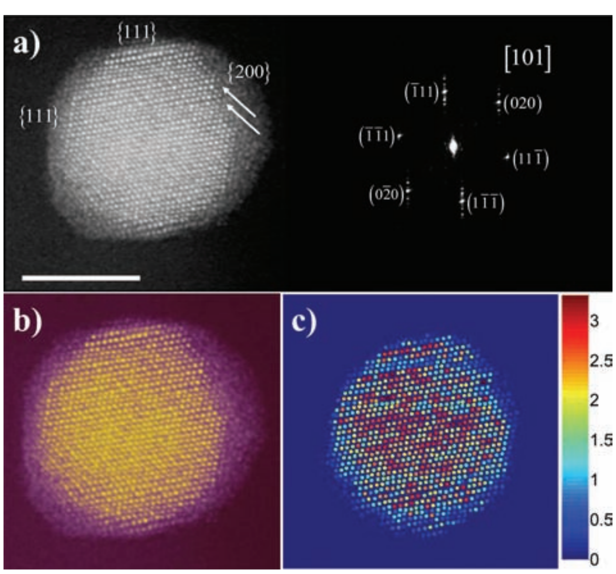

Figure 5. (a) HAADF-STEM image with its corresponding FFT, (b) Color look-up HAADF-STEM image, and (c) Map representing integrated intensity of the atoms.

scattering, it should increase with atomic number (Z) as Z^n where n is expected to be in the range 1.6–1.8,[38] therefore the intensity or contrast of the atomic columns with higher concentration of Pt will be more brighter than the atomic columns with higher concentration of Ni, given that Z of the Pt is 78 and Z of the Ni is 28. The calculation of the integrated intensity was performed assuming that the intensity of the substrate (Carbon film) is equal to zero, and only the contribution of the Pt and Ni atoms was take into account. From the image, the intensity of the atomic column with higher concentration of Pt is well identified from the others, which it has a dark red color in the color map, and also, it is located mixed with the Ni formed an alloy structure.

Most of the nanoparticle of $Ni_{50}Pt_{50}/SiO_2$ catalyst showed different planes, this is really important because it change the properties of the catalyst, each type of property is linking with the kind of atoms in the last layer also the orientation of the nanoparticle is important too. Two NiPt structures can be found,[26] the first one, the planes are mixed by Ni and Pt atoms, according our analysis this typical structure is founded in $Ni_{50}Pt_{50}/SiO_2$, maybe Pt atoms promote the activity of Ni atoms, even this kind of arrangement of atoms were due to the calcinations and reduction, electronic and thermodynamic phenomena are linked with this kind of arrangement. The second one shows a plane rich in Ni atoms, due to the natures of Ni this is less active than the Pt; the Ni atoms cover all the atoms of Pt therefore the properties catalytic change drastically.

According to the development of the catalysis, the active phase actually plays a principal role in many catalytic reactions because it acts as sites that allow the adsorption of different gases and as result, the conversion to products. Actually this active phase usually comprises transition metals because it is more active in its reduce state. However, superficial oxidation of the metal phase possible may have occurred as a result of the atmospheric conditions.

H_2-TPR analysis was conducted to investigate the state of the metallic phases in the monometallic and bimetallic catalyst. Figure 6 illustrates the H_2-TPR profiles obtained, the profile of H_2-TPR reduction showed that the Pt oxide exhibit two small H_2 consumptions peak at temperature of reductions at 370 K and 625 K. In general the peak showed around 325–400 is attributed to the formations of oxides of Pt and the peak at 625 K is attributable to strong interaction metal and support. Hence indicates that this catalysts is not in its reduce state, these oxides could have occurred during the preparations in the incipient wetness impregnation method as we can see in this range of temperature it does not show significantly H_2 consumption peaks.

In the case of catalyst $Ni_{50}Pt_{50}/SiO_2$, the impregnation of Ni in the Pt catalyst resulted due to strong interactions between metal/support in characteristic electronic and physics properties of Ni and Pt on surface of silica. The profile of $Ni_{50}Pt_{50}/SiO_2$ exhibited the first peak of H_2 consumptions at 450 K, this peak could correspond at the PtO and NiO formed during handling or storage of the samples. The principal H_2 consumption peak from 600–750 K signifies that total Ni and Pt reduction occurred during the reduction stage with H_2 even this peak may signify the presence of Pt^{+2} and then Ni^{+2} ions in the form of Ni and Pt oxides. This is because there are some particles of Pt riches in Ni formed as intermetallic nanoparticles and the particles NiO originate from the re-oxidations of metallic Ni formed during reduction. Hence this large peak may be attributed to the size of metal particles of Ni; in this case the size of particle plays an important role in catalysis.[39]

The profile of Ni/SiO_2 showed two H_2 consumptions peaks, the first is positioned at 600 K as been reported to the existence of NiO nanoparticles formed during the preparations of the catalyst also it is attributable to the existence of NiO nanoparticles whit different sizes. Other peaks are formed from 650–800 K, attributable to the presence principally of Ni^{+2} ions in the formation of NiO due to the re-oxidation of nanoparticles whit differences sizes, according with the literature also is consider due to the presence of a kind of phyllosilicates, which occurs by the strong interaction of Ni and SiO_2 support.

The Figure 7 shows the overall N_2O decomposition as a function of the reaction temperature displayed by Ni, Pt and $Ni_{50}Pt_{50}/SiO_2$ catalyst, for the N_2O decomposition, as we can see the activity of the Ni/SiO_2 catalyst to the N_2O decomposition is very low around 20% N_2O decomposition at 900 K, comparing to the literature this catalyst is most better than the other because of its activation energy during the reaction of decomposition of N_2O,[5] nevertheless we were waiting this activity due to the poor Ni characteristics in the catalytic activity, in the case of Pt/SiO_2 catalyst almost 45% of N_2O has been transformed in N_2 and O_2 at 900 K and the total decomposition was around 1005 K, that kind of catalytic activity in the Pt is evident first because is more active than Ni, and second because the particles show planes more actives where the linear triatomic molecule arrives and then this is broken, according our analysis in HR-TEM most of the nanoparticles of Pt showed {111} planes, according to the literature[40] this kind of planes are more actives than the other planes, finally the total conversion is achieved at 1025 K. In the case of $Ni_{50}Pt_{50}/SiO_2$ catalyst the N_2O decomposition is very high more than Pt and Ni, as we can see in the graphic this catalysis started to be active from 740 K this kind of reaction is good because the activation of this catalyst is minimal compared to the Pt and Ni catalysts, actually to reduce the energy is important for many kind of reactions. This result shows that the active surface of $Ni_{50}Pt_{50}/SiO_2$ catalyst is composed for Ni and Pt atoms as we can see in previous, according to the HR-TEM and HAADF-STEM analysis most of the bimetallic nanoparticles were founded showing {111} planes and some surface defects.

The properties the bimetallic nanometric catalyst is often different from that in the bulk,[41] this is correlationated with the particle size, kind of atoms in the last lattice,

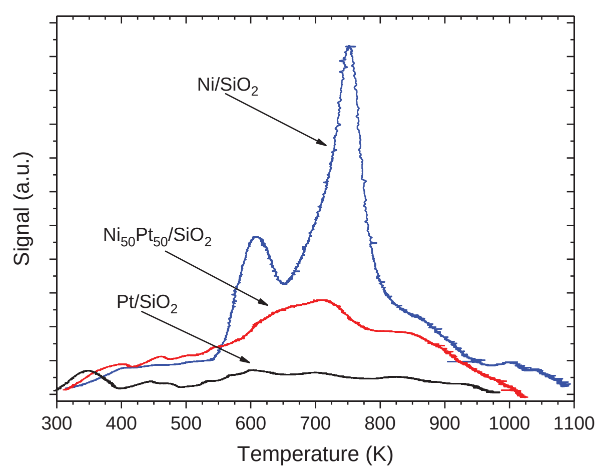

Figure 6. TPR profiles of Ni/SiO_2, Pt/SiO_2 and $Ni_{50}Pt_{50}/SiO_2$ catalysts prepared via incipient wetness techniques.

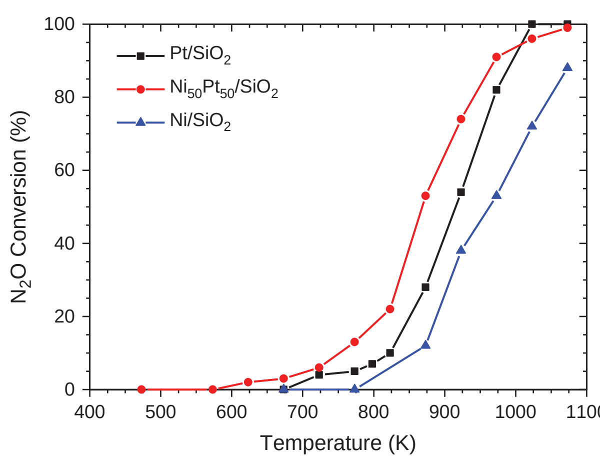

Figure 7. Catalytic activity profiles for catalyst of Ni/SiO_2, Pt/SiO_2 and $Ni_{50}Pt_{50}/SiO_2$ during the decomposition of N_2O gas.

also the kind of planes and direction of the nanoparticle, in our case this kind of phenomena was presented in this catalyst, the size was around 3.5 nanometers, and many particles were founded with cubocataedral shapes, hence the activity of that nanoparticles increase the action of N_2O decomposition. Another reason in the $Ni_{50}Pt_{50}/SiO_2$ is the kind of atoms on the surface, where the surface is mixed with Ni and Pt atoms, in this case the Pt promoted the catalytic activity of the Ni; these kinds of nanoparticles improve the behavior of the catalytic activity in the N_2O decomposition.

It is important to say that when the catalysts are submitted on the thermal treatments in H_2 most of the surfaces are reactivated, in the $Ni_{50}Pt_{50}/SiO_2$ catalyst the surface is enriched in Pt that it promoted the properties in the Ni, while the catalyst is treated in O_2, this allows obtaining nanoparticles in metallic state and regular size. For the N_2O decomposition, first the adsorptions of this molecule takes place in the active surface, then the decomposition of the adsorbed molecule have place and broke the triatomic lineal molecule all this kind of molecules leaving the active surface in form of N_2 and O_2, finally another molecule take place in the active surface, this is another reason why the $Ni_{50}Pt_{50}/SiO_2$ catalyst was more active than the Pt and Ni catalyst.

To understand the behavior of Ni, Pt and NPt particles under dynamic molecular processes, calculations for cuboctahedral configuration were performed. In the Figure 8(a), the plot of the corresponding calculated total energy versus temperature is shown for the cases of Ni, Pt and also for NiPt configurations. As can be observed in the figure, the cooling energy (indicated with red dash-dot lines) is lower in all the systems; however it is interesting to note that with increasing of the Pt content in the structure, the corresponding energy values decrease, therefore the structure becomes more stable. Figure 8(b) shows a sequence of the evolution of the NiPt configuration at different temperatures. The initial configuration is a cuboctahedron with random positions of Ni and Pt. As can be seen, the structure is disordered with increasing of the temperature up to 1400 K, however it is very stable until 800 K approximately. It is important to note that at elevated temperatures, the Ni atoms have a tendency to migrate at the surface of the particle, causing a lower catalytic performance given that more faces with Ni atoms are exposed.

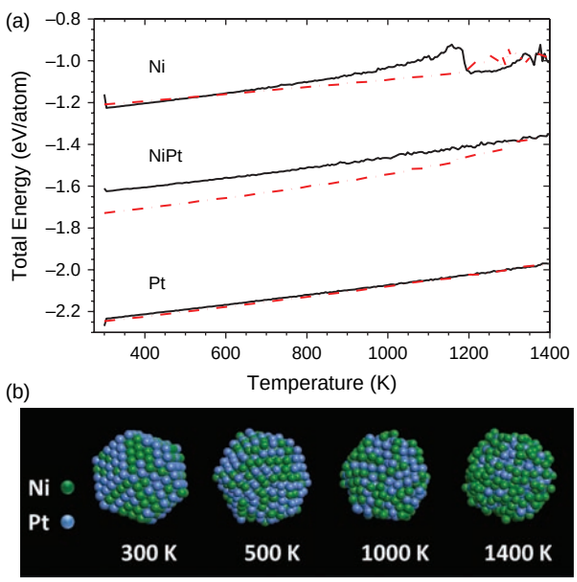

Figure 8. (a) Correlation of the total energies with the temperature of the Ni, NiPt and Pt structures. (b) Models of the NiPt particle at different temperatures.

4. CONCLUSIONS

The properties of monometallic Ni/SiO_2, Pt/SiO_2 and bimetallic $Ni_{50}Pt_{50}/SiO_2$ catalyst were studied using the N_2O decomposition precursor. The result of the analysis of HAADF-STEM shows a good dispersion of the metallic compounds on the SiO_2 support. The analysis for the $Ni_{50}Pt_{50}/SiO_2$ catalyst with 3.5 nm of average size, in specific, this kind of nanoparticles allows to get better N_2O decomposition. One of the principals reason that the nanoparticles has a regular size is because that were oxidized by O_2, in this way we obtained a bimetallic $Ni_{50}Pt_{50}/SiO_2$ in metallic phase, then the H_2 atmosphere allows to react the active phase, electronic and thermodynamic changes occurred in this part of the synthesis, this is one of the reason that the bimetallic catalyst is more active than the monometallic. The analysis of HR-TEM and HAADF-STEM showed the NiPt tetragonal phase and predominantly cuboctahedral shapes with {111} and {020} planes, this kind of planes increased the catalytic activity. The analysis of $Ni_{50}Pt_{50}/SiO_2$ indicated the formation of cuboctahedral particles with planes riches in Ni and Pt mixtures. Due of all characteristics showed, the bimetallic $Ni_{50}Pt_{50}/SiO_2$ catalyst is better than the monometallic catalyst.

Acknowledgments: The authors want to acknowledge to Laboratorio Avanzado de Nanoscopía Electrónica "LANE" at the CINVESTAV-Zacatenco and Dr. Antonio Gómez Cortes at the Institute of Physics of the National Autonomous University of Mexico for the technical support in catalitic analysis.

References and Notes

1. W. Yu, M. D. Porosoff, and J. G. Chen, *Chem. Rev.* 112, 5780 (**2012**).
2. M. Sankar, N. Dimitratos, P. J. Miedziak, P. P. Wells, C. J. Kiely, and G. J. Hutchings, *Chem. Soc. Rev.* 41, 8099 (**2012**).
3. J. Giménez-López, A. Millera, R. Bilbao, and M. U. Alzueta, *Combust. Flame* 157, 267 (**2010**).
4. L. V. Mattos, E. Rodino, D. E. Resasco, F. B. Passos, and F. B. Noronha, *Fuel Process. Technol.* 83, 147 (**2003**).
5. S. Parres-Esclapez, I. Such-Basañez, M. J. Illán-Gómez, C. Salinas-Martínez de Lecea, and A. Bueno-López, *J. Catal.* 276, 390 (**2010**).

6. E. V. Kondratenko, V. A. Kondratenko, M. Santiago, and J. Pérez-Ramírez, *Appl. Catal. B-Environ.* 99, 66 (**2010**).
7. H. Xia, K. Sun, Z. Liu, Z. Feng, P. Ying, and C. Li, *J. Catal.* 270, 103 (**2010**).
8. S. Monyanon, S. Pongstabodee, and A. Luengnaruemitchai, *J. Chin. Inst. Chem. Eng.* 38, 435 (**2007**).
9. W. Essolaani, H. Garbouj, M. Said, F. Picaud, C. Ramseyer, D. Spanjaard, and M. C. Desjonquères, *Surf. Sci.* 603, 2879 (**2009**).
10. P. Légaré, G. F. Cabeza, and N. J. Castellani, *Surf. Sci.* 441, 461 (**1999**).
11. G. Wang, M. A. V. Hove, P. N. Ross, and M. I. Baskes, *Prog. Surf. Sci.* 79, 28 (**2005**).
12. L. E. Murillo, C. A. Menning, and J. G. Chen, *J. Catal.* 268, 335 (**2009**).
13. Ş. Özkara-Aydınoğlu and A. Erhan Aksoylu, *Int. J. Hydrogen Energ.* 36, 2950 (**2011**).
14. N. H. H. Abu Bakar, M. M. Bettahar, M. Abu Bakar, S. Monteverdi, J. Ismail, and M. Alnot, *J. Catal.* 265, 63 (**2009**).
15. K. Nakagawa, S. Takenaka, H. Matsune, and M. Kishida, *Stud. Surf. Sci. Catal.* 175, 793 (**2010**).
16. W. Lonergan, D. G. Vlachos, and J. G. Chen, *J. Catal.* 271, 239 (**2010**).
17. P. Albers, K. Seibold, G. Prescher, and H. Müller, *Appl. Catal. A-Gen.* 176, 135 (**1999**).
18. S. D. Jackson, G. J. Kelly, and G. Webb, *J. Catal.* 176, 225 (**1998**).
19. C. Roth, N. Benker, M. Mazurek, F. Scheiba, and H. Fuess, *Appl. Catal. A-Gen.* 319, 81 (**2007**).
20. J. A. Rodriguez, *Surf. Sci.* 345, 347 (**1996**).
21. G. Wang, H. Wu, D. Wexler, H. Liu, and O. Savadogo, *J. Alloy Compd.* 503, L1 (**2010**).
22. O. Skoplyak, M. A. Barteau, and J. G. Chen, *Surf. Sci.* 602, 3578 (**2008**).
23. L. E. Murillo and J. G. Chen, *Surf. Sci.* 602, 919 (**2008**).
24. T. Wadayama, N. Todoroki, Y. Yamada, T. Sugawara, K. Miyamoto, and Y. Iijama, *Electrochem. Commun.* 12, 1112 (**2010**).
25. C. Wang, M. Chi, G. Wang, D. van der Vliet, D. Li,; K. More, H.-H. Wang, J. A. Schlueter, N. M. Markovic, and V. R. Stamenkovic, *Adv. Funct. Mater.* 21, 147 (**2011**).
26. J. Arenas-Alatorre, M. Avalos-Borja, and G. Díaz, *Appl. Surf. Sci.* 189, 7 (**2002**).
27. A. Gómez-Rodríguez, L. M. Beltrán-del-Río, and R. Herrera-Becerra, *Ultramicroscopy* 110, 95 (**2010**).
28. J. M. Cowley and A. F. Moodie, *Acta Cryst.* 10, 609 (**1957**).
29. J. Hillt and J. Sauer, *J. Phys. Chem.-US* 99, 9536 (**1995**).
30. R. Wang, H. Wang, B. Wei, W. Wang, and Z. Lei, *Int. J. Hydrogen Energ.* 35, 10081 (**2010**).
31. M. V. Sivaiah, S. Petit, M. F. Beaufort, D. Eyidi, J. Barrault, C. Batiot-Dupeyrat, and S. Valange, *Micropor. Mesopor. Mat.* 140, 69 (**2011**).
32. B. Liu, J. H. Chen, X. X. Zhong, K. Z. Cui, H. H. Zhou, and Y. F. Kuang, *J. Colloid. Interf. Sci.* 307, 139 (**2007**).
33. V. Raghavan, *J. Phase Equilib. Diff.* 32, 64 (**2011**).
34. M. D. Graef and M. E. McHenry, Structure of Materials: An Introduction to Crystallography, Diffraction and Symmetry, Cambridge University Press, New York (**2012**).
35. R. Esparza, A. F. García-Ruiz, J. J. Velázquez Salazar, R. Pérez, and M. José-Yacamán, *J. Nanopart. Res.* 15, 1342 (**2013**).
36. A. Mayoral, H. Barron, R. Estrada-Salas, A. Vazquez-Duran, and M. Jose-Yacaman, *Nanoscale* 2, 335 (**2010**).
37. D. Liu, X. Wang, X. Wang, W. Tian, Y. Bando, and D. Golberg, *Sci. Rep.* 3, 1 (**2013**).
38. S. Hillyard and J. Silcox, *Ultramicroscopy* 58, 6 (**1995**).
39. L. Gan, H. Du, B. Li, and F. Kang, *New Carbon Mater.* 25, 53 (**2010**).
40. I. A. Pašti and S. V. Mentus, *Electrochim. Acta* 55, 1995 (**2010**).
41. A. Mayoral, F. L. Deepak, R. Esparza, G. Casillas, C. Magen, E. Perez-Tijerina, and M. Jose- Yacaman, *Micron* 43, 557 (**2012**).

Received: 5 May 2014. Accepted: 11 June 2014.